Brain Topography (2019) 32:897–913
https://doi.org/10.1007/s10548-019-00719-7

ORIGINAL PAPER

# Brain-State Extraction Algorithm Based on the State Transition (BEST): A Dynamic Functional Brain Network Analysis in fMRI Study

Young-Beom Lee[1,2] · Kwangsun Yoo[3] · Jee Hoon Roh[4] · Won-Jin Moon[5] · Yong Jeong[1,2]

Received: 28 December 2018 / Accepted: 28 May 2019 / Published online: 3 June 2019
© Springer Science+Business Media, LLC, part of Springer Nature 2019

## Abstract

Spatial pattern of the brain network changes dynamically. This change is closely linked to the brain-state transition, which vary depending on a dynamic stream of thoughts. To date, many dynamic methods have been developed for decoding brain-states. However, most of them only consider changes over time, not the brain-state transition itself. Here, we propose a novel dynamic functional connectivity analysis method, brain-state extraction algorithm based on state transition (BEST), which constructs connectivity matrices from the duration of brain-states and decodes the proper number of brain-states in a data-driven way. To set the duration of each brain-state, we detected brain-state transition time-points using spatial standard deviation of the brain activity pattern that changes over time. Furthermore, we also used Bayesian information criterion to the clustering method to estimate and extract the number of brain-states. Through validations, it was proved that BEST could find brain-state transition time-points and could estimate the proper number of brain-states without any a priori knowledge. It has also shown that BEST can be applied to resting state fMRI data and provide stable and consistent results.

**Keywords** Brain-state · Transition time-point · Spatial standard deviation · Number of components · Bayesian information criterion · Functional MRI

## Introduction

Brain-state changes dynamically, transitioning from one state to another according to internal or external situations (Baker et al. 2014; Vidaurre et al. 2016). It can, for instance, be expressed as certain activity patterns across the brain on electroencephalograms (EEGs) or functional magnetic resonance imaging (fMRI) (Bassett and Bullmore 2006). In particular, in fMRI studies, early connectivity methods essentially assumed temporal stationarity, i.e. that the brain-state is static for entire data acquisition period (e.g. seed-based correlation analysis (Biswal et al. 1995) and independent component analysis (McKeown et al. 1998a; Kiviniemi et al. 2003; Beckmann et al. 2005). These approaches allowed us to identify brain-states associated with a particular task (Mckeown et al. 1998b), diseases (Lynall et al. 2010; Sanz-Arigita et al. 2010; Hoekzema et al. 2014), or even resting-state (Van De Ven et al. 2004; Meunier et al. 2009). However, because of its origin, they could not reflect the dynamic nature of brain-states.

To date, various methods have been developed to characterize dynamic brain changes. Among those methods, sliding time-window approach has been widely used to decode

Handling Editor: Louis Lemieux.

**Electronic supplementary material** The online version of this article (https://doi.org/10.1007/s10548-019-00719-7) contains supplementary material, which is available to authorized users.

✉ Yong Jeong
yong@kaist.ac.kr

1 Laboratory for Cognitive Neuroscience and NeuroImaging, Department of Bio and Brain Engineering, KAIST, 291 Daehak-ro, Yuseong-gu, Daejeon 34141, South Korea

2 KI for Health Science and Technology, KAIST, 291 Daehak-ro, Yuseong-gu, Daejeon 34141, South Korea

3 Department of Psychology, Yale University, New Haven, CT 06520, USA

4 Department of Neurology, Asan Medical Center, University of Ulsan College of Medicine, 88 Olympic-ro 43-gil, Songpa-gu, Seoul 05505, South Korea

5 Department of Radiology, Konkuk University Medical Center, Konkuk University School of Medicine, 4-12 Hwayang-dong, Gwangjin-gu, Seoul 05030, South Korea

brain-states in terms of the temporal dynamics of fMRI data (Allen et al. 2014). In this method, a time-window of a certain length slides from start- to end-point of the data, with some or no overlaps, and constructs a connectivity matrix on each time-window to express information reflecting the brain-state at that time. Subsequently, a cluster analysis method is applied to connectivity matrices to decode brain-states. Sliding time-window approach has been utilized for dynamic functional connectivity analysis during both task (Bassett et al. 2011; Chai et al. 2016; Telesford et al. 2016) and resting conditions (Hutchison et al. 2013; Barttfeld et al. 2015; de Pasquale et al. 2016; Liu et al. 2016). This approach is easy and intuitive; however, lengths and overlaps between time-windows have been defined arbitrarily, which induces spatiotemporal noises (Shakil et al. 2016). This is even more problematic when applied to resting-state fMRI data (Hindriks et al. 2016), since, in resting-state, it is not possible to know when the internal situation changes. Presumably, durations and transitions of brain-states are not constant, but vary according to cognitive states or characteristics of each individual (Liu et al. 2016; Telesford et al. 2016). Therefore, detecting brain-state transition time-points and defining time-windows based on them might be the necessary step to reduce spatiotemporal noises. Another issue in dynamic functional network analysis is determining the number of brain-states. In many studies, arbitrarily defined number of brain-states also induces unexpected noises. More specifically, when the number of predefined brain-states is small, there is a possibility that two or more brain-states are combined, while a single brain-state will be broken up when using a larger number of brain-states. Therefore, certain criteria is needed to determine the number of brain-states.

To solve these problems, several alternative dynamic functional network analyses have been developed that share a common framework but have different methodological advantages (Thompson and Fransson 2018). In the study (Shine et al. 2016), temporal variation (MTD) is used to divide data into segregated and integrated states and show how states are related to cognitive performance. In the other studies, they tried to detect change points for correlation networks (Barnett and Onnela 2016; Jeong et al. 2016; Ting et al. 2018) only inferring from the data. Another studies used the Hidden Marcov Model to probabilistically infer spatio-temporal patterns of the brain (Baker et al. 2014; Vidaurre et al. 2017) and used a combination of the activations of the ROI at each time as a spatial pattern itself, clustered with predefined numbers, to extract brain-states (Thompson and Fransson 2017). All these studies demonstrated significant results using an alternative method, such as providing good performance or a solution to the original problem of previous dynamic functional network analyses, but at the same time, still reported problems such as adding a hypothesis in terms of methodology for analysis (weight vector in HMM) or having predetermined parameters such as the number of clusters. In order to alleviate these problems, we tried to detect transition time-points through the simplest parameter to reduce another hypothesis and obtain all the results in a data-driven manner without predefined parameters.

Therefore, we propose a novel method for dynamic functional connectivity analysis, termed brain-state extraction algorithm based on the state transition (BEST). First, to detect the transition time-point of the brain-state, we calculated the duration time that a pattern representing a particular brain-state appears as a brain activity map. The BOLD activity pattern is based on the brain-state, and it gradually transitions to another pattern, reflecting another brain-state (Tagliazucchi et al. 2012; Liu and Duyn 2013; Zalesky et al. 2014; Barttfeld et al. 2015). At the time of brain-state transition, the activity would change in brain regions related to the brain-state rather than those not related to the brain-state. Changes of amplitude also can be the feature of change-point of the brain-state (Lindquist et al. 2007), however, it is difficult to apply the spontaneous fluctuation of the resting-state fMRI data since it requires deciding of base-line amplitude. The pattern of the brain-state may change depending on where the baseline is defined in the resting-state fMRI without a priori information related to rest or task blocks. To overcome this limitation, we want to make the absolute value of feature related to the brain-state transition time. In that sense, we focused on the instantaneous SNR of the activity pattern at each time. SNR can be quantified variability of activity pattern as spatial standard deviation (SSD), and we could assume that SSD can be used as a reference value to detect brain-state transition time points. In many studies of EEG microstate, global field power, which is related with SSD, are already being used to find distinct pattern of each microstate (Skrandies 1990; Koenig et al. 2002) which can support our assumptions. Second, we wanted to decode the number of brain-states estimated by the distribution of the connectivity matrices. To this end, we used a cluster analysis method using Bayesian information criterion (BIC), which can quantify the intrinsic complexity of connectivity matrices, depending on the number of brain-states.

To validate brain-state transition time-point detection step, we used fMRI data obtained during performance of a block-designed task with known brain-state transition time-points, and used simulated connectivity matrix dataset constructed from a given number of brain-states to validate brain-state number estimation step. We could show that BEST can detect transition time-points and estimate the proper number of brain-states. Moreover, when BEST were applied to resting-state fMRI data of different sessions from same participants, it could reveal more reliable and consistent results than sliding time-window approach. We have finally applied BEST to resting-state

fMRI data of Alzheimer's disease (AD) patients and have demonstrated that BEST can show differences between patients and healthy controls (HCs) with high specificity and sensitivity.

## Materials and Methods

### Theory

BEST detects transition time-points and makes time-windows between them in order to reduce noises induced by the arbitrarily defined window parameters. This approach enables us to construct each connectivity matrix only within the epoch of the specific brain-state. In order to detect the transition time-point, we focused on the relation between the brain-state and its spatial activity pattern. A brain-state can be represented as a distinct and localized topology pattern (activation map, network, etc.) formed when engaging in a certain task or even in resting-state (e.g. default mode network) and signal-to-noise ratio (SNR) of the brain-state's topology pattern can be quantified with SSD. We hypothesized that, as the brain-state changes (i.e. the topology pattern changes), SSD also changes and the topology pattern at the local peak of SSD time-series will represent the brain-state with the greatest SNR. Furthermore, a topology pattern remains essentially constant between two troughs of the SSD time-series. Therefore, we constructed connectivity matrices those are supposed to represent brain-states in the time-window surrounded by troughs (Fig. 1a) and applied clustering method to the connectivity matrix dataset to decode brain-states (Fig. 1b).

BEST also estimated the appropriate number of brain-states by clustering using BIC (Pelleg and Moore 2000). BIC provides a criterion that is used in the model selection from a Bayesian point of view (Schwarz 1978). In this study, there are two models, one is to maintain the number of brain-states, and the other is to increase the number of brain-states one more. For each of two models, BIC score is calculated as the spatial similarity between all extracted brain-states and the connectivity matrices belonging to those brain-states and a model with a higher BIC score is selected. When the second model is selected and the number of brain-states increases, the connectivity matrix dataset is also divided accordingly and the same step is applied to each sub-dataset. This process repeats until the number of clusters no longer increases.

As far as we know, this is the first time to detect the brain-state transition of fMRI data with SSD and to estimate the brain-state number by clustering using BIC. In the validation section, we confirmed that these approaches could produce consistent and meaningful results.

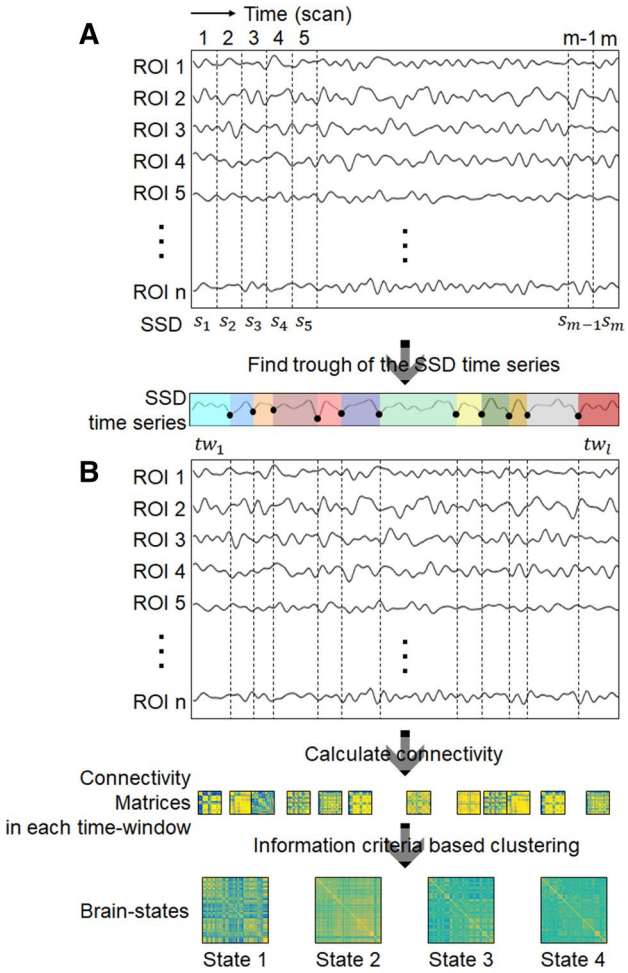


**Fig. 1** The schematics of BEST. **a** In BEST, spatial standard deviation (SSD) based brain-state transition time-point detection was used. SSD were calculated in each fMRI scan, and brain-state transition time-points were detected at the trough of SSD fluctuations. **b** In each time-window (tw), connectivity matrices were constructed. They were used as a dataset of Bayesian information criteria-based clustering approach to decode the representative brain-states

### Detection of Transition Time-Points Using SSD

As previously mentioned, the amplitude of BOLD signal increases locally rather than uniformly in whole-brain areas when the spatial patterns of the brain map become distinct, allowing one to quantify such patterns according to SSD of each time scan. SSD value at time m, $s_m$ is calculated by

$$s_m = \left( \frac{1}{n-1} \sum_{i=1}^{n} \left( x_i - \bar{x} \right)^2 \right)^{\frac{1}{2}},$$

where $n$ is the number of ROIs, $m$ is the scan number, $x_i$ is the averaged BOLD amplitude in the i$^{th}$ ROI, and $\bar{x}$ is the mean value of all $x$. We defined the troughs of the SSD

time-series which has local minimum SNR as the transition time-points and make time-window between each of them. In the SSD time-series, there are some troughs that are little to no distance from the contiguous peak (like saddle points), thus not appropriate for connectivity analysis. We applied various thresholds (from 0 to 0.5) to avoid arbitrariness when detecting the transition time-points. The average SSD value is almost two and we considered that a change of at least 10% would be suitable as a criterion for brain-state transition. Thus, time-points with the min peak prominence of less than 0.2 were discarded.

## Construction of Connectivity Matrices

In each temporal window, Pearson's correlation value, $R_{ij}$, between the time-series of all ROIs pairs was calculated to construct weighted functional connectivity matrices according to the formula for the sample correlation coefficient,

$$R_{ij} = \frac{cov(S_i, S_j)}{\sqrt{var(S_i)var(S_j)}},$$

where $i$, $j$ represents the ROI indices and $S_k$ is the BOLD signal of the k$^{th}$ ROI.

## Decoding Brain-States by Clustering

All connectivity matrices were then used in the clustering method to decode representative brain-states. In each step of clustering method, we considered two candidate models ($M_k,\ K = 1,\ 2$) based upon whether the current dataset would be divided or not ($M_1$ = not divided and stay in one cluster, $M_2$ = divided into two clusters). In each $M_k$, BIC scores, $BIC(M_k)$ were calculated according to

$$BIC(M_k) = \hat{l}_k(D) - \frac{p_k}{2} \cdot \log Q,$$

where $\hat{l}_k(D)$ is the log-likelihood of the windowed connectivity matrix dataset according to the $k^{th}$ model, $p_k$ is the number of parameters in $M_k$, and Q is the number of the connectivity matrices. The term $\hat{l}_k(D)$ was calculated based on the sum of reciprocal of the Euclidean distance between the center of each cluster (=brain-state) and the connectivity matrices within this cluster. A high BIC score indicates that connectivity matrices maintained high similarity within a cluster and low similarity between clusters. We therefore selected the model with the higher BIC score. If model 1 was selected, the data was maintained. When model 2 was selected, the data was divided into two sub-datasets using 2-means clustering. This process was repeated until there were no sub-datasets to be divided. To diminish the effect of initialization problems, we also used k-means ++ algorithm (Arthur and Vassilvitskii 2007) when selecting two initial centroids. We chose the first centroid uniformly at random from among the data points and calculated distances between the chosen centroid and all data points. The next centroid was selected with probability using a weighted probability distribution of distances.

## Validation Experiment 1: Transition Time-Point Detection in Task fMRI Data

We used SSD to detect the brain-state transition time-point. To validate whether the transition time-point can be selected on the appropriate temporal location, we applied BEST to fMRI data obtained from the block designed motor task that could induce "known" brain-state transitions at the beginning of each block. For quantitative analysis, we compared the time-interval between actual transition time-points derived from the task design and detected transition time-points from both task session and control session (without task).

### Participants

Seventeen healthy adults volunteered for fMRI experiment [five women, 12 men; mean age, 22.5 (SD: ± 1.6) years, ranging from 21 to 27 years]. We excluded seven participants because the correlation between their SSD time-series and frame-wise displacement (FD) was significantly high ($r > 0.7$, $p < 0.05$, Supplementary Fig. S1). We therefore utilized fMRI data from 10 participants for validation [three women, seven men; mean age, 22.6 (SD: ± 1.9) years, ranging from 21 to 27 years]. The mean FD values were not significantly different between the task and control group with respect to these ten participants (Supplementary Fig. S2). All participants were right-handed with no history of neurological or psychiatric disorders. Participants provided written informed consent prior to participation in the present study, which was approved by the Institutional Review Board (IRB) of Korea Advanced Institute of Science and Technology. All experiments were performed in accordance with relevant guidelines and regulations.

### Task Experiment

The fMRI experiment was organized into block designed motor task and control sessions (Fig. 2a,b). In the motor task session, participants were asked to clench and unclench their left hands once per second during 10-s time blocks, denoted by a black cross on the screen. Each task block was followed by a 10-s rest period, denoted by a white cross on the screen. Blocks in each session were repeated for 7-min. We acquired fMRI data from same participants without task (control session). During the 7-min,

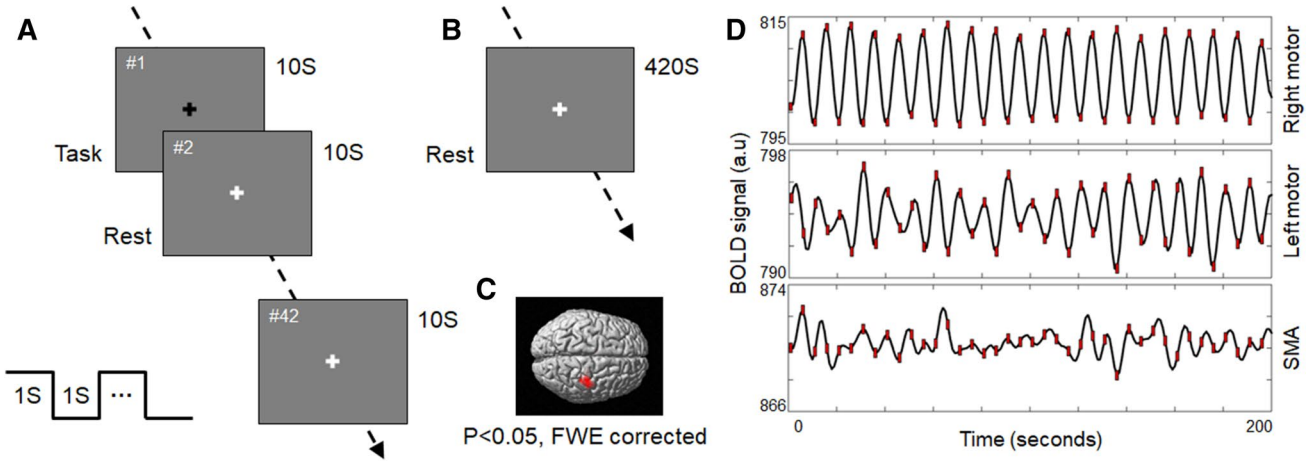


**Fig. 2** Schematic illustration of the fMRI experiment. **a** In the task session, subjects were asked to clench and unclench their left hands repeatedly. **b** Control fMRI data were also acquired over a time period with the same duration as in the task session. **c** Univariate analysis showed that the task induced the expected brain activation in the right primary motor area. **d** Averaged BOLD signal from the right motor area, left motor area, and supplementary motor area. Red markers indicate the start and end time-points of a task block. In the right motor areas, the averaged BOLD signal correlates fully with the task block, with no latency, as compared with the signals from the left motor area and supplementary motor area

participants were asked to keep their eyes open and focus on a fixed black cross at the center of a gray screen.

We observed that right motor regions were activated by the task (Fig. 2c). At the first-level analysis, images of the contrast of the parameter estimates were created for each participant for the effects of interest (task block–rest block) to identify regions preferentially activated by the task. For each effect of interest, contrast images from each participant were entered into a second-level analysis. One-sample t-tests were used to generate statistical parametric maps of the t-statistic at each voxel, allowing identification of voxels demonstrating significant differences in activation between the task and rest. In order to maximize the likelihood of detecting small experimental effects while minimizing false-positive clusters, the threshold for significance for second-level analyses was set at $p < 0.05$, family-wise error corrected for the task experiment with a cluster extent threshold (k) of 100 voxels.

We extracted the BOLD signal from the left and right motor areas as well as the supplementary motor areas for comparison with the block model (Fig. 2d). We observed that the peaks and troughs of the BOLD signal from the right motor area matched well with the block model with about one scan latency. However, the signal from the left motor area was less matched relative to that of the right. In the supplementary motor area, the peaks and troughs of the BOLD signal were not matched with blocks.

### MRI Data Acquisition

The structural and functional images of the task-related experiment were acquired using a 3T MRI scanner (Siemens Magnetom Verio, Germany) with a 32-channel head coil. Functional images with BOLD signals were recorded using a gradient-echo echo planar imaging sequence of 36 axial slices (repetition time (TR) = 2000 ms; echo time (TE) = 30 ms; flip angle = 90°; matrix size = 64 × 64; voxel size = 3 × 3 × 3 $mm^3$). For the structural images, the three-dimensional magnetization-prepared rapid acquisition gradient-echo sequence was used to acquire high spatial-resolution anatomical information (TR = 1800 ms; TE = 2.52 ms; matrix size of the volume data = 256 × 256 × 176).

### Image Preprocessing and Time-Series Extraction

Image pre-processing was performed using SPM12 (Wellcome Trust Centre for Neuroimaging, London, UK, http://www.fil.ion.ucl.ac.uk/spm/software/spm12) and a custom script in MATLAB. The time series of images for each participant were realigned. Images were registered to the first image in the series. All volume slices were corrected for different signal acquisition times by shifting the signal measured in each slice relative to the acquisition of the slice at the mid-point of each TR. Individual structural images were co-registered to the mean functional image. The

transformed structural images were then segmented into gray matter, white matter, and CSF. Then, mean time signals were extracted and regressed out. Head motion is known to have a great effect on measurements of functional connectivity (Power et al. 2012). Therefore, we attempted to diminish the impact of head motion using correction methods. During data preprocessing, we applied motion correction by aligning each functional volume to the reference volume. We then regressed out head motion from the data using a 12-parameter model. Finally, we applied linear de-trending and the band-pass filter (0.001–0.1 Hz).

#### Exclusion of Data Contaminated by Motion Artifacts

Although we regressed out motion-related artifacts during pre-processing, they may have remained if there were large amounts of movement. Therefore, we attempted to discern the extent to which such artifacts influenced fMRI data from each participant. FD is a value that allows for the representation of instantaneous head motion as a scalar quantity (Power et al. 2012). FD was estimated in both task session and control session for each time and used to calculate the correlation with SSD time series in order to determine the influence of noise derived from motion artifacts. Participant data with significantly high correlation ($r > 0.7$, p-value $< 0.05$) between SSD time-series and FD were discarded from each dataset.

#### Region of Interest (ROI)

To focus on changes in functional connectivity in well-known brain networks, we used ROIs related to the intrinsic connectivity network (Shen et al. 2013). However, 268 nodes were originally defined using a group-wise spectral clustering algorithm, we used 244 ROIs because some cerebellar regions were discarded during image acquisition. Nodes were further grouped into eight networks named according to their correspondence to other existing resting-state networks. ROIs were normalized into fMRI data of each participant with transformation parameters from the segmentation step in pre-processing. Figure 3a illustrates an example of a functional connectivity matrix and network ordering. Figure 3b,c visualize topology patterns of two networks (motor network and default mode network) to be analyzed in the subsequent sections.

### Validation Experiment 2: Brain-State Clustering Approach

In order to validate the clustering approach using BIC, we applied it to the simulated connectivity matrix dataset constructed from pseudo brain-states with a known number. States decoded by BEST were compared with original pseudo brain-states.

#### Simulated Data

We constructed four $268 \times 268$ pseudo brain-states. Elements in each pseudo brain-state were defined by randomly selected values from a normal distribution of with a mean of 0 and a SD of 0.3, $N(0, 0.3^2)$. Simulated connectivity matrices were constructed by summing each pseudo brain-state and 100 noises with $N(0, 0.2^2)$. Four hundred connectivity matrices were constructed for validation with a SNR of 1.5 based on the equation

$$STD_{sig}/STD_{noise}$$

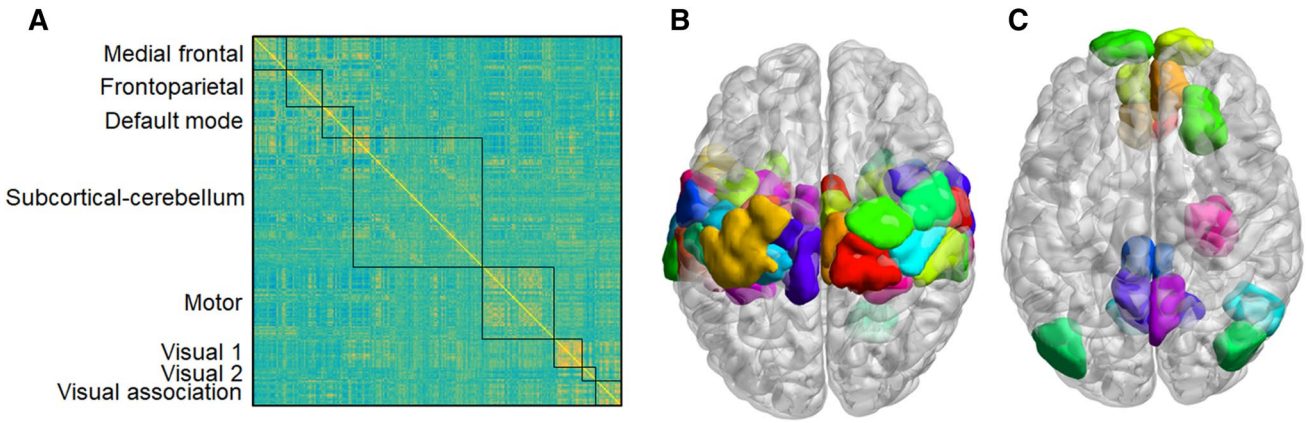


**Fig. 3** Brain network-related regions of interest (ROIs). **a** A total of 268 ROIs were parcellated using a group-wise spectral clustering algorithm. All ROIs were ordered according to the eight brain networks (medial frontal, fronto-parietal, default-mode, subcortical-cerebellum, motor, visual 1, visual 2, and visual association network) using the same clustering algorithm. Among the 268 ROIs, we finally used 244 ROIs, because some cerebellar regions were discarded from image acquisition. **b** ROI visualization of the motor network and **c** default mode network. The cerebellar region of each network was discarded

We also performed validation test even in a null-case situation with no brain-state transition to verify that sampling variability does not result in false positives (Hindriks et al. 2016). We generated a simulation dataset based on the assumption that the connectivity matrices comes from one brain-state without any transition. The pseudo brain-state and connectivity matrices were constructed by using same parameters as those used above. In summary, 100 connectivity matrix dataset were constructed with a SNR of 1.5.

## Validation Experiment 3: Comparison of BEST With Sliding Time-Window/Clustering Approach

We compared the brain-states decoded by BEST and sliding time-window/clustering approach using fMRI data from validation experiment 1. We expected that BEST would more accurately express the different task-dependent brain-state patterns than sliding time-window and clustering method. As participants were required to complete the task with their left hands, increased connectivity should be observed in the right motor area relative to the left (Solodkin et al. 2001; Lindenberg et al. 2013). Therefore, we focused on the laterality of the motor network connectivity and estimated the performance difference between two methods.

### Determination of Parameters for Sliding Time-Window/Clustering Approach

We determined arbitrary parameters for sliding time window/clustering approach similar to those used in BEST. The length of the sliding time-window was determined by the average length of the transition time-window of BEST (eight scans). To maintain similar conditions, each sliding time-window was not overlapped (offset = 0). The number of brain-states was determined using elbow criterion and, as a result, the same numbers used in BEST were also estimated for both task and control sessions.

## Validation Experiment 4: Applicability of BEST to the Resting-State fMRI Data

With the above validations alone, we were not sure if BEST could be applied to the resting-state fMRI data. Therefore, we tried to show that BEST could also decode meaningful brain-states in resting-state fMRI data. Recent studies have shown that resting-state functional connectivity can reflect individual identity (Reineberg et al. 2015; Finn et al. 2017; Gordon et al. 2017) and these specific features are not affected by daily variation (Gratton et al. 2018). BEST therefore was applied to the two sets of resting-state fMRI data acquired at different time-points (acquired once and re-acquired after 4 months) from same participants. We examined whether brain-states were expressed well, and whether the brain-state maintained similar features in both sessions. For quantitative comparison, we compared applicability of BEST and sliding time-window/clustering approach.

### Participants

The ethics committee of each participating institution approved by the IRB at Konkuk University Medical Center, and written informed consent was provided by both participants of the study. All experiments were also performed in accordance with relevant guidelines and regulations. The study included seven healthy subjects (four men and three women; mean age, 30 years; age range, 25–33 years). All the subjects were right handed. The subjects had no history of neurological or psychological diseases, and normal cognitive function was confirmed based on an in-depth interview and mini-mental state examination performed by an experienced neurologist (9 years of experience) at the neurology outpatient clinic.

### Resting-State fMRI Data Acquisition

Each subject was scanned twice using the 3-T MR scanners (Skyra; Siemens, Erlangen, Germany), with a 4 month interval between scans. Multi-channel receive-only coils (16–20 channels) were used in the experiments. During the resting-state acquisitions, no specific cognitive tasks were performed, and the subjects were instructed to close their eyes, minimize their eyeball movements, and relax inside the imager. RS-fMRI data were acquired using a gradient-echo echo-planar imaging (EPI) sequence with the following parameters: TR/TE = 2000/30 ms, field of view (FOV) = 240 mm, number of dynamics = 180, flip angle = 90°, matrix size = 80 × 80, and voxel size = 3 × 3 × 4.5 $mm^3$. T1-weighted anatomical data for the scanners were acquired using a sagittal-oriented magnetization-prepared rapid gradient-echo sequence with the following parameters: TR/TE/inversion time (TI) = 2300/3/900 ms, flip angle = 9°, matrix size = 256 × 256 × 176, and isotropic voxel size = 1 $mm^3$. We applied the same image pre-processing step and ROI for validation as in the task experiment.

## Validation Experiment 5: Applicability of BEST to Individual Data

To extract brain-states from individuals, fMRI data should be obtained over a sufficient length of time because the clustering method should secure a sufficient number of connectivity matrices to construct a proper hyperplane. Therefore, we acquired 35-min of fMRI data using the same paradigm as in validation experiment 1. Four healthy adults volunteered for the fMRI experiment [Three men, one woman; mean age, 22.2 (SD: ± 1.2) years, ranging from 21 to 25 years] to get the long

take task fMRI data. All the validation approaches were the same as those used in validation experiment 1.

### Validation Experiment 6: Applicability of BEST to the AD Data

Finally, we examined whether the brain-states obtained using BEST for clinical resting-state fMRI data of AD patients and HCs reflected the characteristics of the actual etiology.

#### Participants

We included 15 patients with AD with a clinical dementia rating of 1.0 [12 women; mean age: 74.3 (SD: ± 4.4) years, ranging from 67 to 81 years] and 16 age- and education-matched HCs [12 women; mean age: 73.9 (SD: ± 4.2) years, ranging from 67 to 79 years]. Each patient underwent a comprehensive neurological examination, laboratory investigations, neuropsychological testing, and brain MRI. The patients' caregivers were also interviewed. The procedures of this experiment were approved by the IRB at Asan Medical Center, and written informed consent was provided by both participants and caregivers. All experiments were also performed in accordance with relevant guidelines and regulations.

We used the same pre-processing procedures, including those for head motion correction, as previously described for the validation experiments.

#### MRI Data Acquisition

Resting-state fMRI scans of patients with AD as well as HCs were obtained using a 3T scanner (Model: Philips Intera Achieva, Phillips Healthcare, Netherlands). Scans involved the acquisition of 35 axial slices using a gradient echo planar imaging pulse sequence with the following parameters: TR = 3000 ms; TE = 30 ms; FOV [from right to left (RL), from anterior to posterior (AP), and from foot to head (FH)] = 212 × 195 × 160 $mm^3$; voxel size (RL, AP, FH) = 3.31 × 3.31 × 3.31 $mm^3$. During image acquisition, participants were instructed to remain still with their eyes open. T1-weighted anatomical images were also obtained for each participant [TR = 6.8 s; TE = 3.1 s; FOV (RL, AP, FH) = 270 × 270 × 170 $mm^3$, reconstructed voxel size = 1 × 1 × 1 $mm^3$]. ROIs were determined in the same way as in validation experiment 1.

## Results

### Validation Experiment 1: Transition Time-Point Detection in Task fMRI Data

To validate detection of brain-state transition time-points, we applied our method to fMRI data of a block-designed motor task, which allowed us to induce brain-state transitions by block changes. We then measured time-intervals between block changes and detected time-points to demonstrate how well our method can detect brain-state transitions (Fig. 4a). We used results from fMRI data of a control session for quantitative comparison. As a result, time-intervals of task sessions was consolidated to about one scan after the transition time-point, which could be explained by hemodynamic response function (HRF) delay, whereas the time-intervals were widely distributed in the control session (Fig. 4b). The distribution of time-intervals between two sessions were significantly different (unpaired Welch's t-test, $p < 0.0001$), indicating that our method can detect brain-state transition time-points in the task session.

### Validation Experiment 2: Brain-State Clustering Approach

To validate clustering approach, we applied it to the simulated dataset derived from pseudo brain-states with known numbers. Decoded states were then compared with the original pseudo brain-states. Figure 5a shows the constructed pseudo brain-states and simulated connectivity matrices. Eventually, four states were decoded from simulated connectivity matrix dataset and each of these corresponded well to the given pseudo brain-state with high spatial correlation (Fig. 5b). In the case of null situation, one brain-state was also extracted with high spatial correlation (R = 0.9978).

### Validation Experiment 3: Comparison of BEST With Sliding time-Window/Clustering Approach

We compared the brain-states decoded by BEST and sliding time-window/clustering approach with task fMRI data. Using our method, three brain-states were decoded in both task and control sessions (Fig. 6a). To analyze the relationship between brain-states in each session, we calculated the spatial correlations between all possible combinations. The third brain-state in the control session and the second brain-state in the task session exhibited the highest spatial similarity (Fig. 6b, correlation coefficient, r = 0.88). We then isolated the motor network from these sessions (Fig. 6c) and found increased connectivity in areas related to the right motor area in the task session

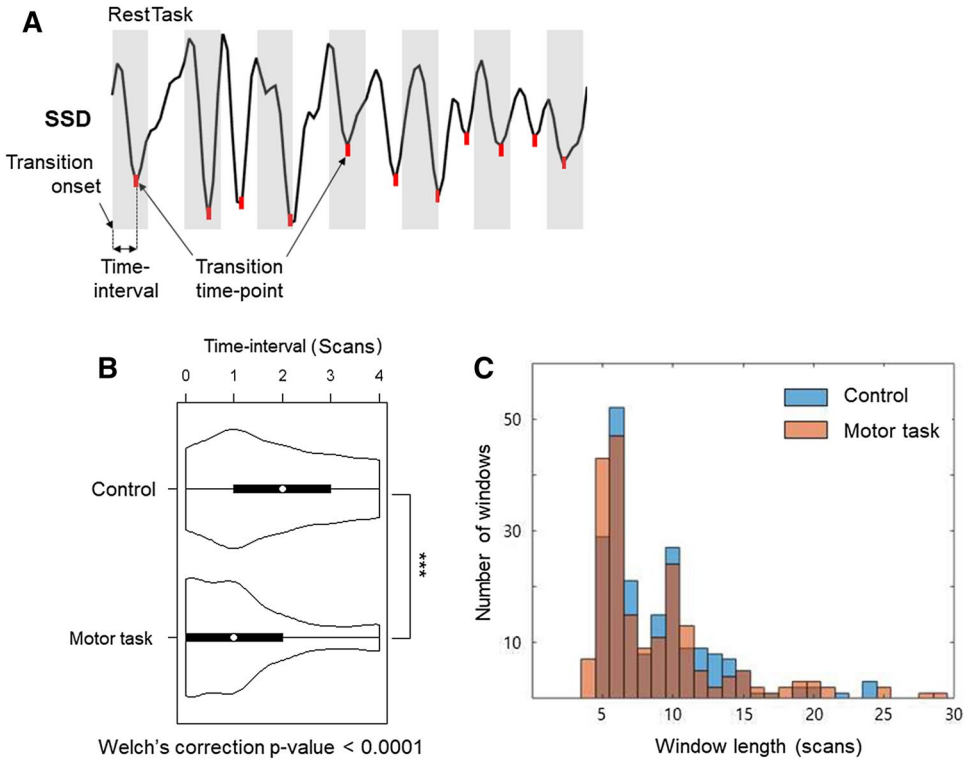


**Fig. 4** BEST can detect task induced brain-state transition time-points. **a** Time intervals between detected transition time-points on the spatial standard deviation (SSD) fluctuations and start point of each block. **b** Time-interval for each session. In the task session, transition time-points are centralized and close to the start point of task blocks, indicating that they are synchronized with the task, whereas those of the control session are not. **c** Window lengths for each session. Unspecified color space is where the histogram of the two sessions overlap. The length of the window was more concentrated in the five scans in the task session than in the control session

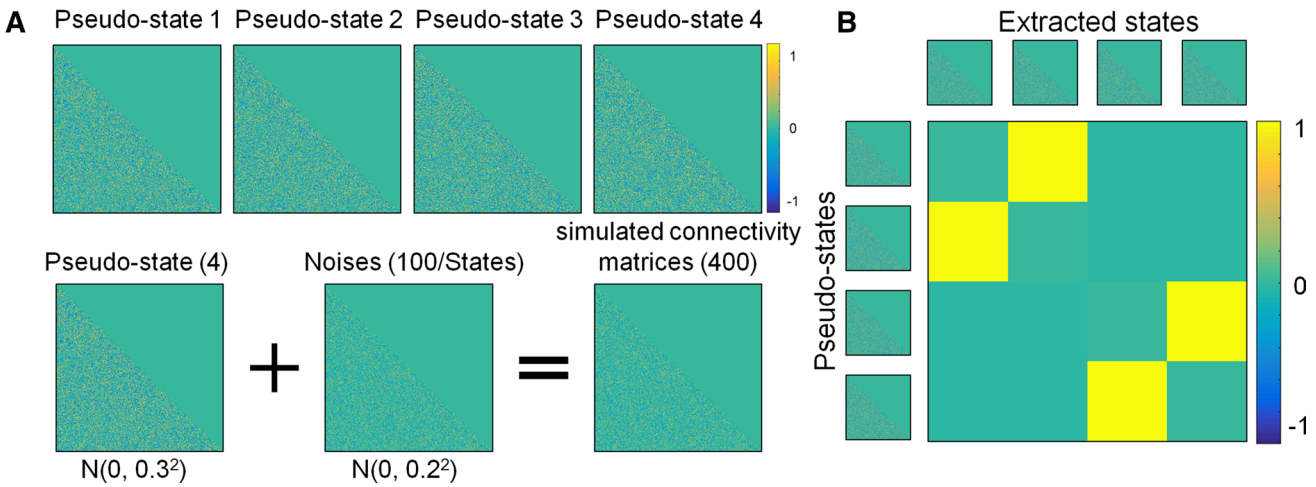


**Fig. 5** BEST can estimate the number of simulated brain-states and decode its spatial pattern. **a** Pseudo brain-states and simulated connectivity matrices. Four hundred simulated connectivity matrices were constructed from four pseudo brain-states combined by 100 noise matrices. **b** A similarity matrix between the original pseudo brain-states and decoded states by BEST. Each unique state corresponds to the specific original pseudo brain-state with high spatial similarity

(Fig. 6d, unpaired t-test, uncorrected $p < 0.0001$). When using sliding time-window/clustering approach, three brain-states were also extracted from both task and control sessions (Fig. 6e). Between motor networks isolated from brain-states with the highest spatial similarity (fig. 6g, state 1 in the resting session, state 1 in the task session), the changes in connectivity due to performance of a motor task were similar to those obtained with BEST. However, more connections between the left motor areas have been found which can be estimated as false-positive due to the nature of the task (Fig. 6h, unpaired t-test, uncorrected $p < 0.0001$).

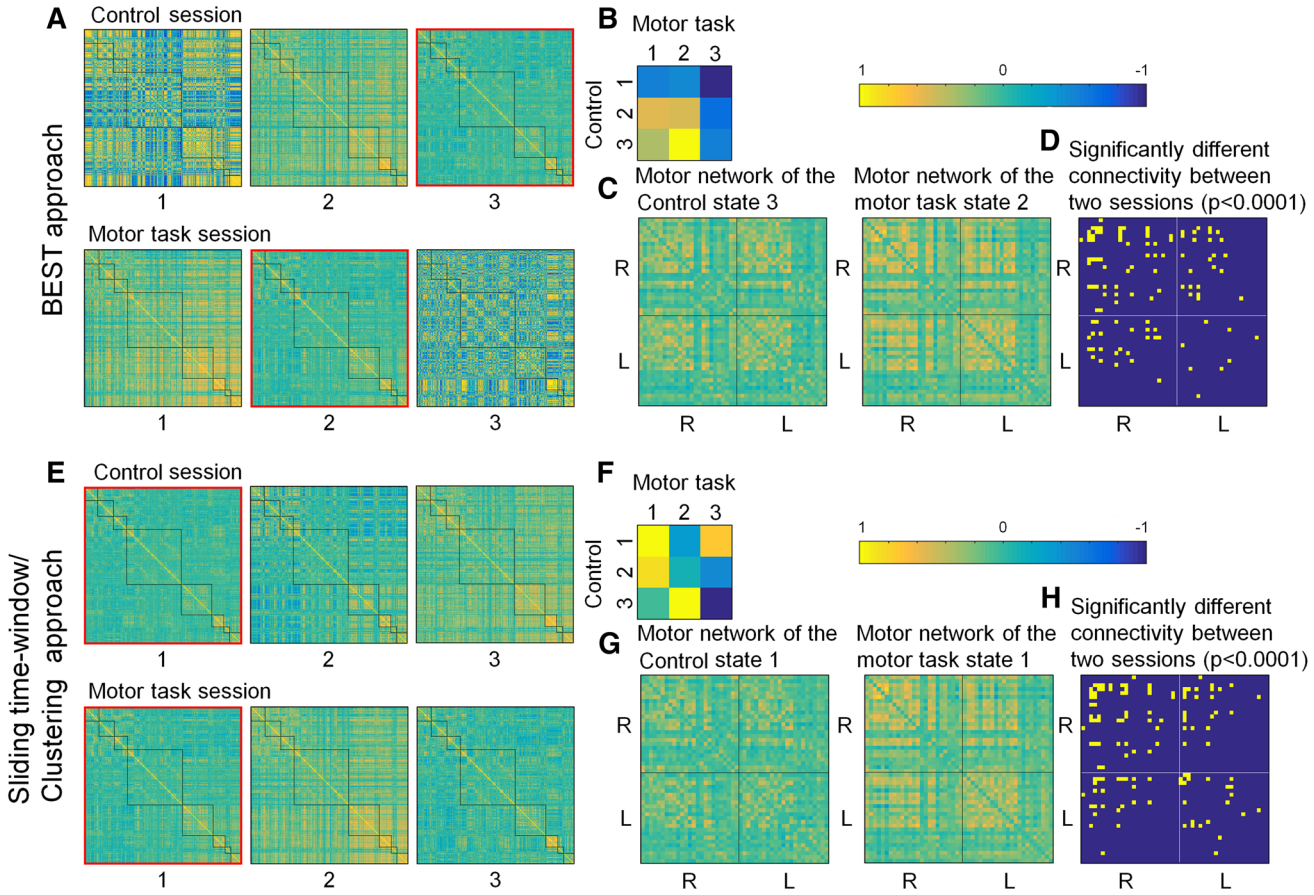


**Fig. 6** Results from BEST is more task-related than those from sliding time-window approach. **a** Decoded brain-states during the motor task and control sessions using BEST. Similar states were constructed in both sessions (states with red borders). **b** A spatial correlation matrix between brain-states in both sessions. **c** Connectivity of the motor network during both sessions. **d** Between the brain-states with the highest spatial correlation, there was significantly increased connectivity values in motor areas during the motor task session (uncorrected t-test, $p < 0.0001$). Most of these are related to the right motor area. **e**. Decoded brain-states during both sessions using the sliding time-window approach. Similar brain-states were constructed in both sessions (states with red borders). **f** A spatial correlation matrix between brain-states from both sessions. **g** Connectivity of the motor network during both sessions. **h** Between the brain-states with the highest spatial correlation, there was significantly increased connectivity values in motor areas during the motor task session (uncorrected t-test, $p < 0.0001$). There are more connectivity changes in the left motor area than seen in the results from BEST

## Validation Experiment 4: Applicability of BEST to Resting-State fMRI Data

To test whether BEST can produce meaningful results in resting-state fMRI data, we applied BEST to two sets of resting-state fMRI data acquired at different time-points, 4 months apart, from same participants. We expected that BEST would decode a consistent pattern of brain-states from different fMRI sessions. As a result, three brain-states were decoded from each of two sessions, and the corresponding brain-states showed high spatial correlations (Fig. 7a,b). We performed same analysis to the results of sliding time-window/clustering approach. We set the number of the brain-states using the elbow criterion. As a result, three brain-states were also decoded in each session, and they showed a relatively low spatial correlation compared to the results derived by BEST (Fig. 7c,d).

## Validation Experiment 5: Applicability of BEST to Individual Data

We decoded two or three brain-states for each individual in both task and control sessions (Fig. 8). We found that there was similar connectivity differences between the two sessions from the group results (validation experiment 3).

## Validation Experiment 6: Applicability of BEST to AD Data

We applied BEST to resting-state fMRI data of AD patients and HCs. As a result, eight brain-states were

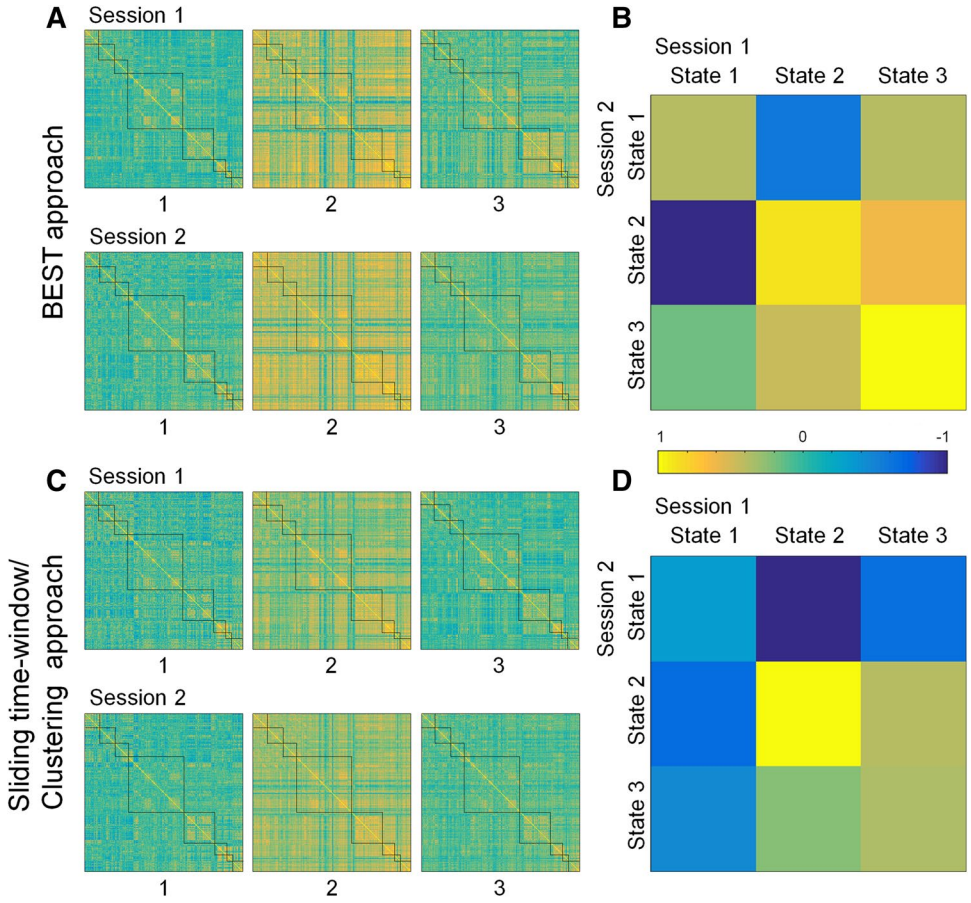


**Fig. 7** BEST can decode highly consistent brain-states from same participants. **a** Brain-states decoded using BEST during the resting session (session 1) and session 2, acquired 4 months after session 1. **b** A spatial correlation matrix between brain-states from session 1 and session 2. **c** Brain-states decoded using the sliding time-window approach. Similar states were constructed in both sessions. **d** A spatial correlation matrix between brain-states from session 1 and session 2. Spatial correlation between corresponding brain-states was higher in the results of BEST than in those of sliding time-window approach

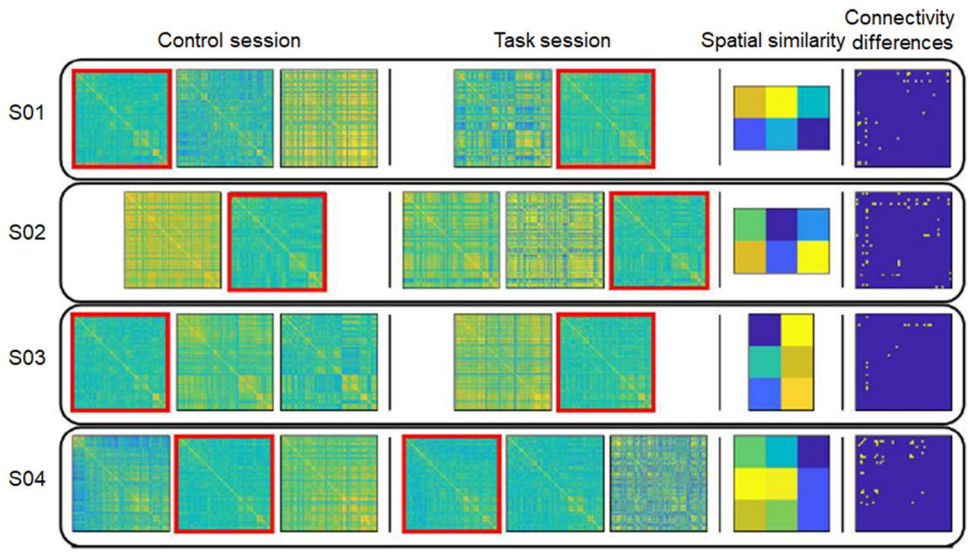


**Fig. 8** Decoded brain-states and connectivity differences arising from individual subject data. A similar number of brain-states is decoded from a single individual's data as from group data. Furthermore, connectivity differences were also detected in connections related with the task ($p < 0.0001$)

extracted from AD group, while five brain-states were extracted from age-matched HC group (Fig. 9a). Shorter time-windows were noted for AD group than HC group ($p = 0.0201$ by t-test, Welch's correction) (Fig. 9e). We calculated the spatial correlations of brain-states between all possible combinations from both groups. The first state of the HC group and the seventh state of the AD group exhibited the highest spatial similarity (Fig. 9b, correlation coefficient, $r = 0.74$). We focused on the default-mode network (DMN; Fig. 9c), as a number of studies have reported that decreased connectivity is observed in the DMN of

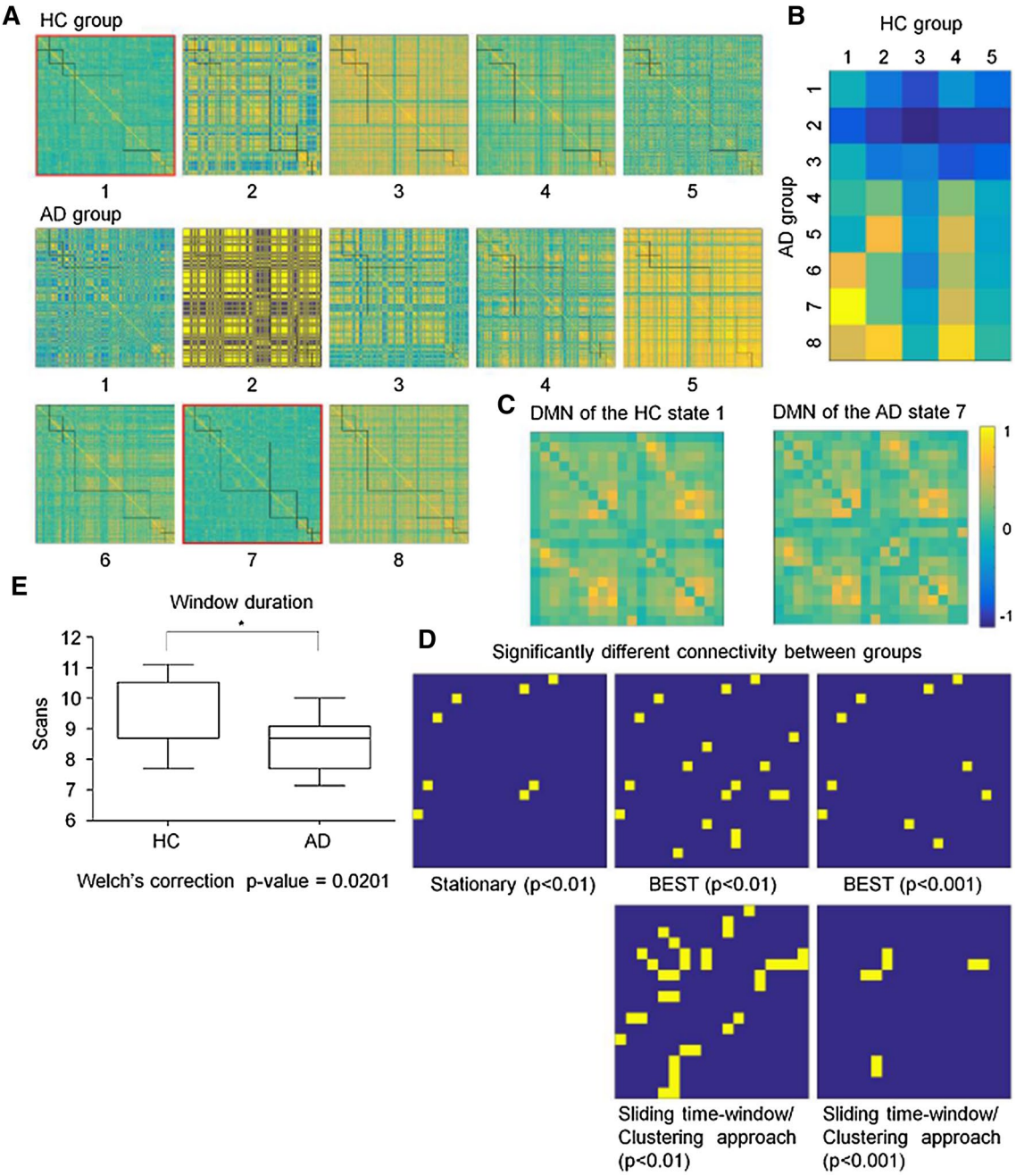


**Fig. 9** Decoded brain-states from healthy control (HC) group and Alzheimer's disease patients (AD) group and its group differences. **a** Brain-states decoded from age-matched HCs and AD groups using BEST. Similar states were constructed in both groups (states with red borders). **b** A spatial correlation matrix between brain-states from HC and AD groups. **c** Connectivity of the default mode network from both groups. **d** There are common connections between the brain-states with the highest spatial correlation (unpaired t-test; p-value < 0.01), which are detected using the stationary connectivity approach (left parietal area—right medial prefrontal area (MPFC), left MPFC—right MPFC, right frontal area—right parietal area, and connectivity between two adjacent MPFCs). When setting significance at a low p-value (p-value < 0.001), there were no significant results when using the stationary connectivity approach; on the other hand, BEST revealed similar results, except for a few connections. **e** Duration of time-windows for the HC and AD groups. In the AD group, brain-states had a shorter duration

patients with AD (Greicius et al. 2004; Supekar et al. 2008; Zhou et al. 2008; Zhang et al. 2009).

Then, we applied same analysis to brain-states extracted by using sliding time-window/clustering approach and results from BEST and sliding time-window/clustering approach were compared with brain-states from a stationary approach. When comparing the results obtained with BEST and those obtained with the stationary approach, BEST could find more differences in the connectivity between the AD group and the HC group than with the stationary approach (Fig. 9d, upper row, middle) at the same significance level of $p < 0.01$. Moreover, the difference in connectivity found by BEST included all the differences in connectivity found by the stationary approach. The results of sliding time-window/clustering approach also included the results of the stationary approach and found more differences (Fig. 9d, lower row, middle). However, spatial patterns of results from two approaches significantly different, and it became more apparent when the stringent statistical threshold ($p < 0.001$) was used. In the case of BEST, most of connectivity differences which were also detected by the stationary approach with low statistical thresholds were maintained [left parietal area—right medial prefrontal area (MPFC), left MPFC—right MPFC, right frontal area—right parietal area, and connectivity between two adjacent MPFCs]. One connection that was not included in the results was the connection between the adjacent left MPFC (Fig. 9d, upper row, right). On the other hand, results of sliding time-window/clustering approach showed no similarity with the results of stationary approach. Different connectivity which were also detected by using stationary approach was not maintained at a high p-value (Fig. 9d, lower row, right), indicating that false-positive results may have been included. From these results, we can conclude that BEST and sliding time-window/clustering approach could detect differences between HC group and AD group with high sensitivity, but the latter had relatively lower specificity, which could lead to bias in interpreting the results.

## Discussion

In this study, we propose a novel approach to dynamic functional connectivity analysis, BEST, for decoding brain-states in fMRI data. It consists of two approaches that can characterize the brain-state. Firstly, it defined the duration of brain-states by detecting transition time-points using SSD and constructed very specific connectivity matrices based on each brain-state. Secondly, BEST estimated number of brain-states that best represents the underlying distribution of connectivity matrices by the clustering method using BIC.

Previous methods have decoded brain-states with connectivity matrices mainly constructed by using sliding time-windows of an arbitrarily defined length and offset. Thus, constructed connectivity matrices could not guarantee inclusion of information of a particular brain-state, since the length and the offset of the sliding time-window is determined without reflecting dynamic characteristics of the brain-states. Therefore, configuring the connectivity matrix by using sliding time-window approach inevitably results in noise generation (Shakil et al. 2016). To overcome these limitations, we attempted to detect brain-state transition time-points and make time-window between them to obtain information about the particular brain-states in a data-driven manner. We hypothesized that SNR of the activity pattern could reflect brain-state transitions and it could be quantified by SSD of activity pattern at each time-point.

We validated SSD based brain-state transition time-point detection approach by applying BEST to fMRI data of two different sessions, the task and control session. In the task session, there are identifiable brain-state transition time-points according to block changes (whether task-to-rest or rest-to-task). On the other hand, in the control session, there are no identifiable brain-state transition time-points because there are no block changes. If our approach can detect time-points of the brain-state transitions, results of task session should be related with task blocks. On the contrary, in the control session, detected time-points would not be related with the blocks of the task session. We show the quantified results in Fig. 4b. The time-interval between detected time-points and task-induced transition onset is converged to one scan (2 s reflecting HRF) in task session and they are widely distributed with no convergence in the control session. We also obtained results of applying the other transition time-point detection method (Ting et al. 2018). In results, the same tendency was observed although the difference was not significant ($p = 0.3147$, Supplementary Fig. S3). This confirmed that the detected transition time-points with BEST reflected the brain-state transition well. We also found that the time-window lengths varied in both sessions (Fig. 4c). Furthermore, we also showed that in the task session, more values were associated with the size of the experimental block (10 s = 5 scans). Transitions of the brain-states in the flow of thought will probably occur at variable intervals, and these results will reflect that aspect.

In the image processing field, it is well known that an approach using various sizes of windows estimated by the data-driven method can be useful for effectively grasping basic information of irregularly distributed data (Egiazarian et al. 2001). In the case of dynamic functional connectivity analysis methods, many studies have used a fixed sliding time-window length. It was suggested that the length of the sliding time-window should be inversely proportional to the frequency cut-off of the high pass filter (Leonardi and Van De Ville 2015). This quantifies the likelihood that the information associated with a brain-state with a dynamic pattern

of low frequency bands may not be expressed in the sliding time-windows with a certain small length. This problem is due to the fixed length of the sliding time-window. In the dynamic functional connectivity analysis with a fixed sliding time-window, there is no base information about the brain-state (e.g. frequency) and researchers have no choice but to estimate. However, since BEST applied the time-window after transition time-point detection, it could apply a small window to the duration of brain-state with a high frequency band and vice versa. The paper (Saggar et al. 2018) showed that the transition of the brain-state occur rapidly and that these patterns can be found in data similar to those used in our paper [TR (1.5 s), 0.009 Hz < f < 0.08 Hz band pass filter].

In this paper, for both the task and control sessions, the average length of the time-window was about eight scans (16 s), which was sufficient to represent brain-states (Gonzalez-Castillo et al. 2015; Saggar et al. 2018). However, a connectivity matrix constructed from a small time-window still might not reflect the brain-states adequately, due to the high sampling variability. To validate whether the connectivity matrices from the small time-window can reflect brain-states, we first generated two connectivity matrix groups based on the length of the windows (upper 25% and lower 25%). We then compared the spatial correlation calculated between connectivity matrices and their brain-states in each group, but found no statistically significant differences between the two groups (Supplementary Fig. S4). We concluded that connectivity matrices obtained from a small time-window would also reflect brain-states, as well as those obtained from a long time-window.

In the dynamic functional connectivity analysis, it is important to define the number of brain-states. However, we do not know how many brain-states exist during the entire time of data collection, especially at rest without tasks. Therefore, clustering approaches, which assume the number of the brain-states arbitrarily, may cause erroneous integration or segregation of the brain-states. To avoid this problem, various approaches have been used to estimate the number of brain-states, for example, elbow criterion (Allen et al. 2014). Elbow criterion approach may validate the proper number of the brain-state. However, elbow criterion doesn't usually work well for some data sets because the criterion value is monotonically decreases. The number estimated by elbow criterion requires manual determination of the number from the clustering validation graph with arbitrary threshold.

We attempted to infer the number of brain-states based on the distribution of connectivity matrices. To solve this problem, we used BIC score to estimate the number of brain-states (Fraley and Raftery 1998; Pelleg and Moore 2000). It has a clear criterion at each step (to divide the cluster, or not); therefore, there was no need to determine ambiguous information (e.g. the curvature of the graph). We obtained near-optimal clustering results with a minimum number of clusters with long inter-cluster distances and short intra-cluster distances. To validate this approach, we constructed pseudo-random brain-states and created connectivity matrices by adding white noises, and decoded brain-states from these connectivity matrices. The number of brain-states estimated by BEST was the same as the given number of pseudo brain-states. Moreover, the spatial correlation between pseudo-states and extracted states was very high (Fig. 5). To verify that sampling variability does not result in a false positive, we also have tested with the null hypothesis assuming that the data is stationary data. As a result, it was confirmed that one brain-state was extracted with high spatial correlation coefficient value. Thus, a cluster analysis method based on BIC is an appropriate approach for estimating the number of brain-states. Connectivity matrices constructed in each participant were also consistent in the same group. To measure the variability, we used similarity between connectivity matrix and its centroid (= brain-state). Similarity was quantified by spatial correlation and we compared the distribution of similarity of all participants. We found no significant differences among participants (see the Supplementary Fig. S5).

Through these validations, we demonstrated that BEST worked well in time-point detection and estimation of the number of brain-states. We then applied BEST to block-designed task fMRI data and compared its performance with that of sliding time-window/clustering approach. When participants performed a motor task with their left hand, the connectivity associated with contralateral right motor areas increased. It is well known that when participants perform a motor task with their left hand, the connectivity associated with contralateral right motor areas increases (Solodkin et al. 2001; Lindenberg et al. 2013). Both approaches detected increased connectivity in the motor areas, although more lateralized connectivity to right motor areas was observed in the case of BEST (Fig. 6d,h). Such findings suggest that BEST is more specific for detecting changes in brain-states during the task session than sliding time-window approach.

Another issue in validating BEST was whether it could be used in resting-state fMRI data. We applied BEST to two sessions of resting-state fMRI data acquired at different time from same participant group. In Fig. 7, we compared brain-states decoded by BEST and by sliding time-window/clustering analysis. The corresponding brain-states from BEST showed high spatial correlation. Sliding time-window/clustering approach, however, failed to decode similar brain-states. It is unclear whether people experience similar brain-states every day, as brain-states could change according to the individuals' physical or mental circumstance; however, presumably, each individual has a predominant and stable brain-state during rest (Gratton et al. 2018), and our method seems to extract these states.

We did not apply an overlap between time-windows when we used sliding time-window/clustering approach in the validation session. Since time-window overlapping might have an effect on the results, we applied the overlapped sliding time-window to the validations. We also yielded consistent results using overlapped time-windows (Supplementary Figs. S6,S7).

Recently, it has been emphasized that fMRI data should be analyzed at individual-level because it can be used to distinguish each individual (Finn et al. 2015; Sohn et al. 2015; Reineberg and Banich 2016; Tavor et al. 2016). We demonstrated that BEST could be applied to an individual's fMRI data. The number of connectivity matrices to use for each individual was problematic, because an insufficient number of estimated brain-states could be obtained with the conventional scan time (5–10 min). Thus, the distribution of the connectivity matrices offered scant information for determining the hyperplane. To acquire a sufficient number of connectivity matrices, we obtained 35 min' fMRI data with the same block-design motor task (Fig. 8). Although a longer duration may be better, the length of fMRI scanning needed to obtain a sufficient number of connectivity matrices is unclear. We obtained about 200 connectivity matrices from 7 min' fMRI data in each participant, and we determined that the amount of time required for obtaining about 100 connectivity matrices from an individual's fMRI data was (28 min + alpha). Thus, brain-states can be decoded from these matrices, and were similar to the group results (increased connectivity associated with right motor areas). We therefore concluded that BEST could be used to for analysis of an individual's brain-states when data is acquired for a sufficiently long period.

Lastly, we applied BEST to resting-state fMRI data of AD patients to assess differences between an AD and HC datasets (Fig. 9). We focused on the decreased connectivity in the DMN regions, which are known to be closely related to AD progression (Greicius et al. 2004; Wang et al. 2006; Wu et al. 2011; Koch et al. 2012). Briefly, BEST and sliding time-window/clustering approach detected more decreased connectivity in the AD patient group than the stationary method under the same p-value ($p < 0.01$). This leads to increasing both true and false positives, which guarantee that the results of the dynamic connectivity analysis methods have a higher sensitivity and lower specificity compared with the stationary analysis method. With a stringent statistical threshold ($p < 0.001$), the stationary method showed no differences in connectivity, while BEST and sliding time-window/clustering approach still showed decreased connectivity. However, the results from sliding time-window/clustering approach were markedly different from those from the stationary approach, while results from BEST included most of the decreased connectivity from the stationary approach. Under the stricter threshold ($p < 0.001$), the stationary analysis method could not detect any significant differences between the two groups, while the two dynamic methods detected decreased connections. In detail, BEST could detect most of connections that were detected by stationary methods with a high p-value. It maintained true positives and decreased false positives, which led to similar sensitivity and greater specificity. When we applied sliding time-window approach, detected connections were not related with the results of stationary approach with high p-value, leading to the decrease of true positives and increase of false positives, which led to a decrease in both sensitivity and specificity. Moreover, the only one exclusion from BEST results was connection between adjacent MPFC possibly due to type 1 error. It is plausible that the brain-state of the stationary approach has relatively less temporal information than those of a dynamic approach; therefore, the former method might fail to detect slightly different connectivity (low sensitivity). However, the connectivity detected using the stationary approach is highly likely to be accurate (high specificity). The results of sliding time-window approach had high sensitivity, but might not guarantee high specificity, while BEST can show results with relatively higher sensitivity, while maintaining specificity, compared to the stationary approach.

BEST also has some limitations. First, it is not a full data-driven method. We determined troughs of SSD using the min peak prominence to 0.2 because the average SSD value is almost two and a change of at least 10% is suitable as a criterion for a brain-state transition. To validate whether this value is suitable as a threshold, we extracted brain-states with various thresholds and compared the similarities between the dominant brain-states by applying each threshold (Supplementary Fig. S8). In the results, the dominant brain-state without threshold is not stable compared with others with thresholds. We concluded that using differentiation (without threshold) is not effective in detecting brain-state transition points. We may be able to solve this through signal normalization methods (e.g. smoothing) in future studies. Second, we hypothesized that brain-states undergo transition with little to no overlap. Such an assumption enables us to assume that fMRI data from each period reflect only one specific brain state. However, in reality, more than two brain-states may interact simultaneously. Future studies should focus on decomposing the SSD time-series to a number of brain-states and elucidating the duration and pattern of each brain-state.

In conclusion, we proposed a novel dynamic functional connectivity network analysis, BEST, which can decode brain-states in a data-driven way, without a priori knowledge. Moreover, it can be applied to both resting-state and task-related fMRI data, with more sensitivity and specificity than existing methods. We expect that this approach will be able to elucidate dynamic features of functional networks in fMRI data for both clinical and research purposes.

**Acknowledgements** This study was supported by grant HI14C2768 from the Korea Health Technology Research and Development Project through the Korea Health Industry Development Institute, funded by the Ministry of Health &Welfare, Republic of Korea.

## References

Allen EA, Damaraju E, Plis SM et al (2014) Tracking whole-brain connectivity dynamics in the resting state. Cereb Cortex 24:663–676

Arthur D, Vassilvitskii S (2007) K-means++: the advantages of careful seeding. Proc Annu ACM-SIAM Symp Discret Algorithms. https://doi.org/10.1145/1283383.1283494

Baker AP, Brookes MJ, Rezek IA et al (2014) Fast transient networks in spontaneous human brain activity. Elife 2014:1–18. https://doi.org/10.7554/eLife.01867

Barnett I, Onnela JP (2016) Change point detection in correlation networks. Sci Rep 6:1–11. https://doi.org/10.1038/srep18893

Barttfeld P, Uhrig L, Sitt JD et al (2015) Signature of consciousness in the dynamics of resting-state brain activity. Proc Natl Acad Sci 112:887–892. https://doi.org/10.1073/pnas.1515029112

Bassett DS, Bullmore E (2006) Small-world brain networks. Neuroscientist 12:512–523. https://doi.org/10.1177/1073858406293182

Bassett DS, Wymbs NF, Porter MA et al (2011) Dynamic reconfiguration of human brain networks during learning. Proc Natl Acad Sci 108:7641–7646. https://doi.org/10.1073/pnas.1018985108

Beckmann CF, Deluca M, Devlin JT, Smith SM (2005) Investigations into resting-state connectivity using independent component analysis. Philos Trans R Soc London B 360:1001–1013. https://doi.org/10.1098/rstb.2005.1634

Biswal B, Yetkin FZ, Haughton VM, Hyde JS (1995) Functional connectivity in the motor cortex of resting human brain using echo-planar MRI. Magn Reson Med 34:537–541. https://doi.org/10.1002/mrm.1910340409

Chai LR, Mattar MG, Blank IA et al (2016) Functional network dynamics of the language system. Cereb Cortex. https://doi.org/10.1093/cercor/bhw238

de Pasquale F, Della Penna S, Sporns O et al (2016) A dynamic core network and global efficiency in the resting human brain. Cereb Cortex 26:4015–4033

Egiazarian K, Katkovnik V, Astola L (2001) Adaptive window size image denoising based on ICI rule. 2001 Proc IEEE Int Conf Acoust Speech Signal Process (Cat No. 01CH37221) 3:1869–1872. https://doi.org/10.1109/icassp.2001.941308

Finn ES, Shen X, Scheinost D et al (2015) Functional connectome fingerprinting: identifying individuals using patterns of brain connectivity. Nat Neurosci 18:1664–1671. https://doi.org/10.1038/nn.4135

Finn ES, Scheinost D, Finn DM et al (2017) Can brain state be manipulated to emphasize individual differences in functional connectivity? Neuroimage 160:140–151. https://doi.org/10.1016/j.neuroimage.2017.03.064

Fraley C, Raftery AE (1998) How many clusters? Which clustering method? Answers via model-based cluster analysis. Comput J 41:578–588. https://doi.org/10.1093/comjnl/41.8.578

Gonzalez-Castillo J, Hoy CW, Handwerker DA et al (2015) Tracking ongoing cognition in individuals using brief, whole-brain functional connectivity patterns. Proc Natl Acad Sci 112:8762–8767. https://doi.org/10.1073/pnas.1501242112

Gordon EM, Laumann TO, Adeyemo B et al (2017) Individual-specific features of brain systems identified with resting state functional correlations. Neuroimage 146:918–939. https://doi.org/10.1016/j.neuroimage.2016.08.032

Gratton C, Laumann TO, Nielsen AN et al (2018) Functional brain networks are dominated by stable group and individual factors, not cognitive or daily variation. Neuron 98:439–452. https://doi.org/10.1016/j.neuron.2018.03.035

Greicius MD, Srivastava G, Reiss AL, Menon V (2004) Default-mode network activity distinguishes Alzheimer's disease from healthy aging: evidence from functional MRI. Proc Natl Acad Sci 101:4637–4642. https://doi.org/10.1073/pnas.0308627101

Hindriks R, Adhikari MH, Murayama Y et al (2016) Can sliding-window correlations reveal dynamic functional connectivity in resting-state fMRI? Neuroimage 127:242–256. https://doi.org/10.1016/j.neuroimage.2015.11.055

Hoekzema E, Carmona S, Ramos-Quiroga JA et al (2014) An independent components and functional connectivity analysis of resting state FMRI data points to neural network dysregulation in adult ADHD. Hum Brain Mapp 35:1261–1272. https://doi.org/10.1002/hbm.22250

Hutchison RM, Womelsdorf T, Gati JS et al (2013) Resting-state networks show dynamic functional connectivity in awake humans and anesthetized macaques. Hum Brain Mapp 34:2154–2177

Jeong SO, Pae C, Park HJ (2016) Connectivity-based change point detection for large-size functional networks. Neuroimage 143:353–363. https://doi.org/10.1016/j.neuroimage.2016.09.019

Kiviniemi V, Kantola J-H, Jauhiainen J et al (2003) Independent component analysis of nondeterministic fMRI signal sources. Neuroimage 19:253–260. https://doi.org/10.1016/S1053-8119(03)00097-1

Koch W, Teipel S, Mueller S et al (2012) Diagnostic power of default mode network resting state fMRI in the detection of Alzheimer's disease. Neurobiol Aging 33:466–478. https://doi.org/10.1016/j.neurobiolaging.2010.04.013

Koenig T, Prichep L, Lehmann D et al (2002) Millisecond by millisecond, year by year: normative EEG microstates and developmental stages. Neuroimage 16:41–48. https://doi.org/10.1006/nimg.2002.1070

Leonardi N, Van De Ville D (2015) On spurious and real fluctuations of dynamic functional connectivity during rest. Neuroimage 104:430–436. https://doi.org/10.1016/j.neuroimage.2014.09.007

Lindenberg R, Nachtigall L, Meinzer M et al (2013) differential effects of dual and unihemispheric motor cortex stimulation in older adults. J Neurosci 33:9176–9183. https://doi.org/10.1523/JNEUROSCI.0055-13.2013

Lindquist MA, Waugh C, Wager TD (2007) Modeling state-related fMRI activity using change-point theory. Neuroimage 35:1125–1141. https://doi.org/10.1016/j.neuroimage.2007.01.004

Liu X, Duyn JH (2013) Time-varying functional network information extracted from brief instances of spontaneous brain activity. Proc Natl Acad Sci 110:4392–4397. https://doi.org/10.1073/pnas.1216856110

Liu F, Wang Y, Li M et al (2016) Dynamic functional network connectivity in idiopathic generalized epilepsy with generalized tonic-clonic seizure. Hum Brain Mapp. https://doi.org/10.1002/hbm.23430

Lynall M-E, Bassett DS, Kerwin R et al (2010) Functional connectivity and brain networks in schizophrenia. J Neurosci 30:9477–9487

Mckeown MJ, Makeig S, Brown GG et al (1998a) Analysis of fMRI data by blind separation into independent spatial components. Hum Brain Mapp 6:160–188. https://doi.org/10.1002/(SICI)1097-0193(1998)6:3%3c160:AID-HBM5%3e3.0.CO;2-1

McKeown MJ, Jung T-P, Makeig S et al (1998b) Spatially independent activity patterns in functional MRI data during the Stroop color-naming task. Proc Natl Acad Sci 95:803–810. https://doi.org/10.1073/pnas.95.3.803

Meunier D, Achard S, Morcom A, Bullmore E (2009) Age-related changes in modular organization of human brain functional networks. Neuroimage 44:715–723

Pelleg D, Moore A (2000) X-means: Extending K-means with efficient estimation of the number of clusters. In: Proceedings of the 17th International Conference on Machine Learning, pp 727–734

Power JD, Barnes KA, Snyder AZ et al (2012) Spurious but systematic correlations in functional connectivity MRI networks arise from subject motion. Neuroimage 59:2142–2154

Reineberg AE, Andrews-Hanna JR, Depue BE et al (2015) Resting-state networks predict individual differences in common and specific aspects of executive function. Neuroimage 104:69–78. https://doi.org/10.1016/j.neuroimage.2014.09.045

Reineberg AE, Banich MT (2016) Functional connectivity at rest is sensitive to individual differences in executive function: a network analysis. Hum Brain Mapp 37:2959–2975. https://doi.org/10.1002/hbm.23219

Saggar M, Sporns O, Gonzalez-Castillo J et al (2018) Towards a new approach to reveal dynamical organization of the brain using topological data analysis. Nat Commun 9:1–14. https://doi.org/10.1038/s41467-018-03664-4

Sanz-Arigita EJ, Schoonheim MM, Damoiseaux JS et al (2010) Loss of "small-world" networks in Alzheimer's disease: graph analysis of fMRI resting-state functional connectivity. PLoS ONE. https://doi.org/10.1371/journal.pone.0013788

Schwarz G (1978) Estimating the dimension of a model. Ann Stat 6:461–464. https://doi.org/10.1214/aos/1176344136

Shakil S, Lee C-H, Keilholz SD (2016) Evaluation of sliding window correlation performance for characterizing dynamic functional connectivity and brain states. Neuroimage 133:111–128. https://doi.org/10.1016/j.neuroimage.2016.02.074

Shen X, Tokoglu F, Papademetris X, Constable RT (2013) Groupwise whole-brain parcellation from resting-state fMRI data for network node identification. Neuroimage 82:403–415

Shine JM, Bissett PG, Bell PT et al (2016) The dynamics of functional brain networks: integrated network states during cognitive task performance. Neuron 92:544–554. https://doi.org/10.1016/j.neuron.2016.09.018

Skrandies W (1990) Global field power and topographic similarity. Brain Topogr 3:137–141

Sohn WS, Yoo K, Lee YB et al (2015) Influence of ROI selection on resting functional connectivity: an individualized approach for resting fMRI analysis. Front Neurosci 9:1–10. https://doi.org/10.3389/fnins.2015.00280

Solodkin A, Hlustik P, Noll DC, Small SL (2001) Lateralization of motor circuits and handedness during finger movements. Eur J Neurol 8:425–434. https://doi.org/10.1046/j.1468-1331.2001.00242.x

Supekar K, Menon V, Rubin D et al (2008) Network analysis of intrinsic functional brain connectivity in Alzheimer's disease. PLoS Comput Biol. https://doi.org/10.1371/journal.pcbi.1000100

Tagliazucchi E, Balenzuela P, Fraiman D, Chialvo (2012) Criticality in large-scale brain fMRI dynamics unveiled by a novel point process analysis. Front Physiol. https://doi.org/10.3389/fphys.2012.00015

Tavor I, Jones OP, Mars RB et al (2016) Task-free MRI predicts individual differences in brain activity during task performance. Science 352:216–220. https://doi.org/10.1126/science.aad8127

Telesford QK, Lynall M-E, Vettel J et al (2016) Detection of functional brain network reconfiguration during task-driven cognitive states. Neuroimage 142:198–210

Thompson WH, Fransson P (2017) Spatial confluence of psychological and anatomical network constructs in the human brain revealed by a mass meta-analysis of fMRI activation. Sci Rep 7:1–11. https://doi.org/10.1038/srep44259

Thompson WH, Fransson P (2018) A common framework for the problem of deriving estimates of dynamic functional brain connectivity. Neuroimage 172:896–902. https://doi.org/10.1016/j.neuroimage.2017.12.057

Ting CM, Ombao H, Samdin SB, Salleh SH (2018) Estimating dynamic connectivity states in fMRI using regime-switching factor models. IEEE Trans Med Imaging 37:1011–1023. https://doi.org/10.1109/TMI.2017.2780185

Van De Ven VG, Formisano E, Prvulovic D et al (2004) Functional connectivity as revealed by spatial independent component analysis of fMRI measurements during rest. Hum Brain Mapp 22:165–178. https://doi.org/10.1002/hbm.20022

Vidaurre D, Quinn AJ, Baker AP et al (2016) Spectrally resolved fast transient brain states in electrophysiological data. Neuroimage 126:81–95. https://doi.org/10.1016/j.neuroimage.2015.11.047

Vidaurre D, Abeysuriya R, Becker R et al (2017) Discovering dynamic brain networks from big data in rest and task. Neuroimage. https://doi.org/10.1016/j.neuroimage.2017.06.077

Wang L, Zang Y, He Y et al (2006) Changes in hippocampal connectivity in the early stages of Alzheimer's disease: evidence from resting state fMRI. Neuroimage 31:496–504. https://doi.org/10.1016/j.neuroimage.2005.12.033

Wu X, Li R, Fleisher AS et al (2011) Altered default mode network connectivity in Alzheimer's disease—a resting functional MRI and Bayesian network study. Hum Brain Mapp 32:1868–1881. https://doi.org/10.1002/hbm.21153

Zalesky A, Fornito A, Cocchi L et al (2014) Time-resolved resting-state brain networks. Proc Natl Acad Sci 111:10341–10346

Zhang HY, Wang SJ, Xing J et al (2009) Detection of PCC functional connectivity characteristics in resting-state fMRI in mild Alzheimer's disease. Behav Brain Res 197:103–108. https://doi.org/10.1016/j.bbr.2008.08.012

Zhou Y, Dougherty JH Jr, Hubner KF et al (2008) Abnormal connectivity in the posterior cingulate and hippocampus in early Alzheimer's disease and mild cognitive impairment. Alzheimers Dement 4:265–270

**Publisher's Note** Springer Nature remains neutral with regard to jurisdictional claims in published maps and institutional affiliations.